JOURNAL OF AIRCRAFT
Vol. 35, No. 4, July–August 1998

Appraisal of Numerical Methods in Predicting the Aerodynamics of Forward-Swept Wings

G. Lombardi* and M. V. Salvetti†
University of Pisa, Pisa 56126, Italy
and
M. Morelli‡
CSIR, Pretoria 0001, South Africa

The capabilities of different numerical methods in evaluating the aerodynamic characteristics of a forward-swept wing in subsonic and transonic flow are analyzed. The numerical results, obtained by means of potential, Euler, and Navier–Stokes solvers, are compared with experimental data. In particular, attention is focused on the aerodynamic quantities related to pressure distributions. Moreover, an attempt is made to investigate the capability of a Navier–Stokes solver to predict separation lines; both laminar Navier–Stokes equations and Reynolds-averaged equations with a k-ε model are considered. This analysis is carried out by comparing the numerical velocity field to the experimental visualizations, obtained through liquid crystals. All of the numerical solvers give results consistent with the physical limits of the equations that they discretized.

Nomenclature

b = span, m
C_L = wing lift coefficient
C_l = sectional lift coefficient
C_M = wing pitching moment coefficient
C_m = sectional pitching moment coefficient
c = local chord, m
c_p = pressure coefficient, $(p - p_\infty)/q_\infty$
M = freestream Mach number
p = pressure
p_∞ = freestream pressure
q_∞ = freestream dynamic pressure
x = distance from wing section leading edge, m
y = spanwise distance from wing root, m
α = angle of attack, deg

Introduction

IMPROVEMENTS in computer-processing speed and storage capacity allowed computational fluid dynamics to become an increasingly powerful tool in the aerodynamic design of aircraft. At the present time, several numerical solvers, based on physical models of different complexity, are available for the evaluation of the aerodynamic loads. Many applications of different numerical methods to aeronautical configurations can be found in the literature.

From a practical point of view, a distinction can be made between inviscid and viscous models. Among the inviscid models, the well-stated linear potential flow solvers are limited to subsonic or supersonic flows. However, extended potential models have been proposed for transonic flows (for instance the fully potential method in Ref. 1). Many examples of numerical solutions of the Euler equations can also be found in the literature.[2,3]

The coupling of an inviscid simulation with a boundary-layer equation solver, e.g., Ref. 4 for an application to the flow over swept wings, can be considered the simplest model accounting for viscous effects. The thin-layer approximation of the Reynolds-averaged Navier–Stokes equations is extensively used for this type of flow, as, for instance, in Ref. 5 for isolated wings and in Refs. 6 and 7 for wing–canard and wing–fuselage configurations, respectively. Finally, the full Reynolds-averaged, Navier–Stokes equations can be solved (for aeronautical applications see, e.g., Refs. 8 and 9).

Clearly, a simplified model can give good results only if the basic physical assumptions are satisfied for the considered body geometry and flow conditions. Moreover, the amount of information provided by such models is limited. On the other hand, the requirements in storage and time increase considerably with the complexity of the method. In the perspective of the application of numerical methods to the aerodynamic design of aircraft, a critical point is the identification of the model giving the desired accuracy with the minimum cost, for each flow condition and for each project phase.

The purpose of this paper is to analyze the accuracy of solvers of different complexities in the evaluation of the aerodynamic characteristics of a high-aspect-ratio, forward-swept wing. This wing configuration is very interesting from the aerodynamic point of view because it increases aerodynamic efficiency, improves low-speed handling, reduces approach speed, and gives better stall/spin characteristics.[10] Moreover, recent developments in the various technological fields have opened the way to a more extensive use of forward-swept wings. An accurate appraisal of the capability and accuracy of the different numerical methods in predicting aerodynamic quantities could yield a significant improvement in the study of forward-swept wing behavior. Indeed, numerical simulation allows the analysis of the flow around such configurations to be carried out faster and at a lower cost than in experiments. Moreover, numerical simulation could provide quantities that are difficult or impossible to measure experimentally.

To obtain a deeper understanding of the real aerodynamic behavior of these configurations, experimental tests were carried out in the Medium Speed Wind Tunnel of the Aerotek Division of the Council for Scientific and Industrial Research (CSIR) facilities, both in subsonic and transonic regimes.[11] An analysis of the experimental measurements of the pressure field

Received Dec. 29, 1995; presented as Paper 96-0289 at the AIAA 34th Aerospace Sciences Meeting, Reno, NV, Jan. 15–18, 1996; revision received Jan. 5, 1998; accepted for publication Jan. 9, 1998.

*Assistant Professor, Department of Aerospace Engineering. Member AIAA.
†Assistant Professor, Department of Aerospace Engineering.
‡Research Engineer, Medium Speed Wind Tunnel.

acting on the wing surface was carried out.[12] Furthermore, from surface flow visualizations, laminar-to-turbulent flow transition and separation lines were identified for different conditions.[13]

This significant amount of experimental data can be used for an accurate appraisal of the real capabilities of the various numerical methods generally used in the different phases of the aerodynamic design of aircraft. Therefore, in the present paper, the experimental results are compared to those obtained by means of numerical methods based on different physical models.

Concerning inviscid models, a potential flow method and an Euler solver are considered. The limits and the accuracy of linear potential flow solvers are well established. Hence, the potential flow results are used here to investigate if the Euler solver can give significant improvements for configurations in which potential methods can also be employed, as, for instance, typical subsonic cruise conditions. Moreover, although the Euler equations neglect viscous terms, they are capable of describing rotational flows, such as the formation of a free shear-layer from the sharp edge of an aerodynamic surface or transonic flows with strong shock waves. Therefore, Euler results are compared with experimental data in transonic conditions. In addition, from a numerical point of view, the performance of a code in Euler computations is the first step in checking a numerical method that can be applied, eventually, to the solution of the Navier–Stokes equations.

To simulate highly separated flows, the solution of the Reynolds-averaged, Navier–Stokes equations is needed. A critical point is the modeling of Reynolds stresses. The sensitivity of the solution to the turbulence model is shown, for instance, in Ref. 14. In our opinion, the capabilities of a Navier–Stokes method in predicting highly separated flows are strongly related to the correct evaluation of the transition lines, but it is known that the closure methods currently used in literature do not give a satisfactory prediction. In this work both laminar Navier–Stokes equations and Reynolds-averaged equations with a k-ε model are considered. This is a first step to check the numerical method, in the perspective of the analysis of current turbulence models capabilities, when the transition line is imposed.

Experimental Setup

The tests were carried out in the Medium Speed Wind Tunnel of the CSIR facilities in South Africa. This is a closed-circuit, pressurized tunnel, with a confined square test section of 1.5 m width and 4.5 m length, enclosed in a plenum. The test section is symmetrically slotted with five tapered soda-bottle-shaped slots per wall, giving a 5% porosity. The Reynolds number can be controlled by pressurizing the tunnel. The behavior of the wind tunnel with respect to blockage is very satisfactory, as can be seen from the analysis of the blockage in the dedicated tests described in Ref. 15, where the main flow characteristics in the test section are also reported.

The wing model[12] in Fig. 1 has zero twist and dihedral angles, a negative sweep angle ($\Lambda = -25$ deg, at one-quarter of the chord), a semispan of 0.7 m, an aspect ratio of 5.7, a taper ratio of 0.4, and wing sections of NACA 0012.

To evaluate the pressure distribution, pressure ports were fitted on the model to obtain a total of 320 measurement points, with 10 span stations and 32 chord points (Fig. 1). The formulation of the error analysis, both for positioning and pressure measurements, has been described in Ref. 11, where the dimensional control carried out on the shape of the wing model and on the position of the orifices is also reported.

The flow visualizations were carried out by means of the liquid-crystal technique, following the procedure described in Ref. 16. By analyzing the changes in the reflected color, details of boundary-layer transition, flow separation, or shock position can be observed.

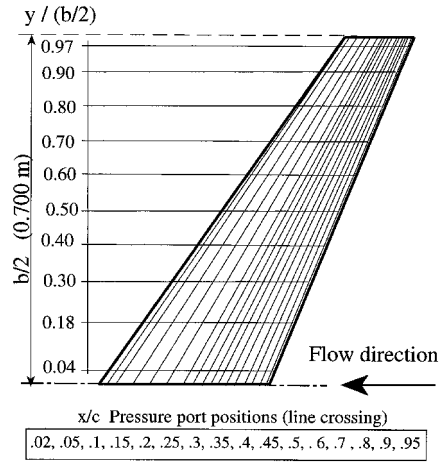

Fig. 1 Definition of the wing model and pressure taps position.

Two flow regimes were chosen for the tests: 1) a subsonic regime ($M = 0.3$) and 2) a transonic regime ($M = 0.7$). By changing the stagnation pressure, the Reynolds number was kept the same ($\approx 2.8 \times 10^6$, based on the mean aerodynamic chord) at both Mach numbers. Tests were carried out for angles of attack up to 28 deg.

The force coefficients were evaluated by means of numerical integration of the pressure distributions. The global lift and pitching moment coefficients (referred to 25% of the mean aerodynamic chord) are nondimensionalized with the freestream dynamic pressure, the wing planform surface, and the mean aerodynamic chord. The sectional lift and pitching moment coefficients along the span (referred to the 25% of the local chord), are nondimensionalized with the freestream dynamic pressure and the local chord. Positive values of the moment coefficients indicate nose-up moments.

Numerical Methods

Different numerical codes, using, respectively, the linear potential flow hypothesis, Euler, and Navier–Stokes solvers, are considered.

The compressible potential flow solver[17] is based on a boundary-element formulation, and its capabilities with respect to the prediction of the aerodynamic loads on complete aircraft were assessed, for instance, in Ref. 18.

For the numerical solution of Euler and Navier–Stokes equations the commercial code RAMPANT[19] (developed by FLUENT) is used. Three- or two-dimensional compressible Euler, Navier–Stokes, or Reynolds-averaged Navier–Stokes equations can be solved. Two turbulence models are available in the RAMPANT code: the standard k-ε model and the renormalization group k-ε model. The numerical method is based on a finite volume formulation applicable to structured or unstructured solution-adaptive grids. The numerical inviscid fluxes are evaluated by Roe's flux-difference splitting.[20] A second-order spatial accuracy is obtained by a Taylor-series expansion in the evaluation of the variables at the cell faces. Steady solutions are obtained by time-marching the equations with an explicit, multistage, Runge–Kutta scheme with multigrid convergence acceleration. A single iteration consists of a complete multigrid cycle. Different orders of time accuracy can be obtained by changing the number of stages in the Runge–Kutta scheme.

All of the simulations are carried out on a Digital Alpha 2100 computer, with a 640 Mbytes RAM. Unstructured grids are used in the Eulerian and Navier–Stokes simulations. The external boundary is represented by a cylinder of circular section, with a radius of 6.75 mean aerodynamic chord and a spanwise length of 2.5 wingspan. At the external boundary, Mach number and static conditions are specified. An analysis of the sensitivity to the dimensions of the computational do-

main was carried out, indicating that, for the domain used here, the influence of external boundary conditions on the solution is negligible. Because of the symmetry of the problem, only the semiwing has been considered and symmetry conditions are imposed at the wing root. The solution is considered converged after a three order of magnitude reduction of the rms residual for each of the conserved variables.

Results of Inviscid Simulations

A first analysis was carried out in subsonic conditions at a freestream Mach number of 0.3. In Fig. 2 the global values of lift and pitching moment, obtained from potential flow, Eulerian calculations, and experiments are plotted as a function of α. More precisely, in this paper we report the values of $-C_M/C_L$, giving an evaluation of the lift point of application. As expected, the potential solution gives a global value of the lift, that is in very good agreement with the experiments for low angles of attack, up to about 10 deg. Because vortical effects and stall phenomena cannot be accounted for by this type of method, the C_L for higher angles of attack is overestimated.

The global lift values obtained from Eulerian simulations are in good agreement with the experiments, even if slightly underestimated, up to an angle of attack of about 12 deg, a condition in which the lift curve is no longer linear. The vortical effects become more important when increasing the angle of attack. It has been assessed in the literature that Euler methods, although limited by the inviscid flow assumption, can simulate the formation of a free shear layer from the sharp edge of an aerodynamic surface. As expected, the agreement is poor for higher angles of attack, when a large part of the boundary layer is separated.

With reference to the spanwise lift distribution in typical cruise conditions, both solvers give a very good agreement with experimental data, as shown, for instance, in Fig. 3a.

In Eulerian simulations the global pitching moment is noticeably overestimated for all angles of attack, as can be seen from Fig. 2b.

The spanwise distribution at a typical cruise condition (Fig. 3b) also indicates that the lift application point obtained by Eulerian calculations is located downstream of the experimental one. This discrepancy appears because in Eulerian simulations the pressure peak at the leading edge is underestimated, as shown, for instance, by the chordwise pressure distribution at 40% of the wing span, plotted in Fig. 4. This is because of errors related to the spatial discretization. Because the zone near the leading edge is characterized by high gradients of the flow variables, the solution is extremely sensitive to the local grid resolution. Moreover, the amount of numerical viscosity introduced by the upwind method used here also depends on the grid resolution. The gap between the experimental data and the Eulerian results is reduced when the computational grid is refined. As an example, in Fig. 5 the chordwise pressure distribution at the same section as described earlier is plotted for three different unstructured grids

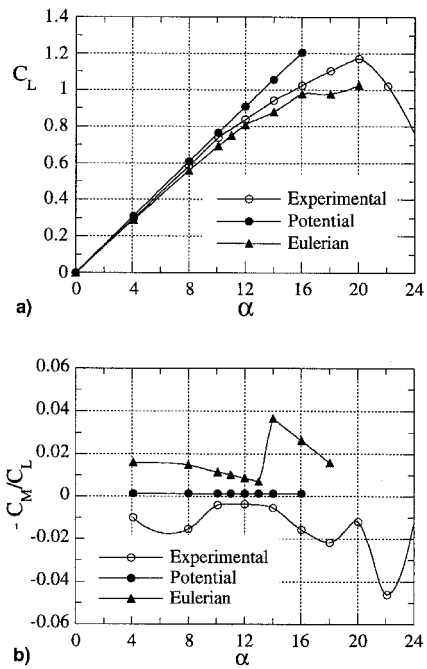

Fig. 2 Global values; M = 0.3: a) lift curve and b) estimation of the lift point of application.

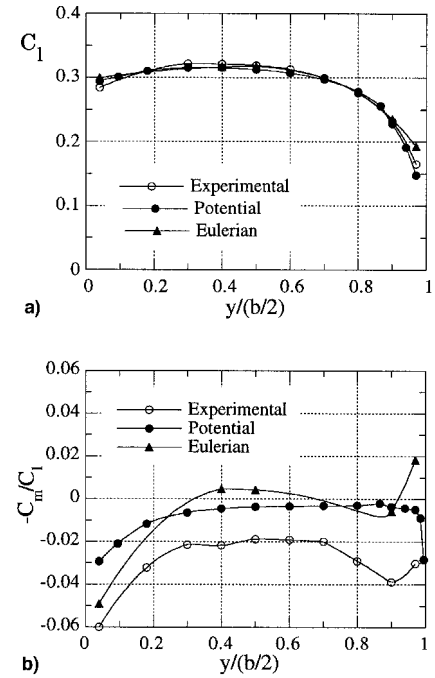

Fig. 3 Spanwise distributions; M = 0.3 and C_L = 0.296: a) lift distribution and b) estimation of the lift point of application.

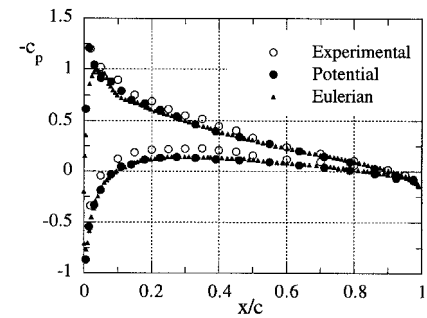

Fig. 4 Chordwise pressure distribution; M = 0.3, α = 4 deg, and $y/(b/2)$ = 0.4.

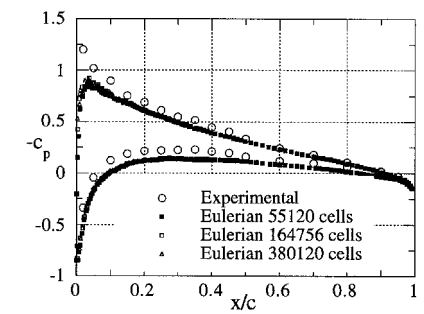

Fig. 5 Effect of the mesh refinement in Eulerian solution; M = 0.3, α = 4 deg, and $y/(b/2)$ = 0.4.

of 55,120, 164,756, and 380,120 tetrahedral cells, respectively. The grids are locally refined around the leading edge, on the wing and in the domain. The agreement with experimental data in the prediction of the suction peak is improved with the grid refinement, but it is still not satisfactory. In particular, the differences between the peak values obtained with the 164,756 and 380,120 cell grids are negligible. The results presented in this section for Euler computations are obtained with the mesh of 164,756 cells and the CPU time needed, for each simulation at $M = 0.3$ is about 10 h. All of the CPU times given in this paper are not systematically optimized and must be taken only as an indication. For the potential flow calculations 600 panels are used on the semi-wing and a few seconds of CPU time are required for one simulation. Although this coarse discretization, the potential flow solver gives a better evaluation of the leading-edge pressure peak (Fig. 4). As a result the global pitching moment shows a better agreement with the experimental data (Fig. 2b). The spanwise distribution in Fig. 3b shows that the Eulerian qualitative trend of the lift point of application is in better agreement with the experimental data.

As previously mentioned, the global lift values obtained by Eulerian simulations are in good agreement with experimental data also when the C_L is no longer linear with α. To investigate if this globally good agreement is also obtained locally, in Fig. 6a the lift spanwise distribution is shown for a C_L corresponding to an angle of attack close to 12 deg. A good agreement with the experimental data is found in the spanwise distribution, except near the wing root. Indeed, as pointed out in Ref. 11, at this angle of attack the flow near the wing root is not attached. However, it should be pointed out that, in this region, the experimental results could be affected by the effects of the sidewall boundary layer,[21,22] whereas in the numerical simulations, symmetry conditions are imposed at the wing root. This behavior is confirmed by the analysis of the pitching moment spanwise distribution in Fig. 6b, where a large gap between Eulerian results and experimental data is found at the wing root. A better qualitative agreement is observed when moving toward the tip.

To investigate the capabilities of the Eulerian flow solver in transonic conditions, a second set of comparisons was carried out at a freestream Mach number of 0.7.

In Fig. 7 the global values of lift and pitching moment obtained from Eulerian computations are compared to experimental data for different angles of attack. The global lift is well predicted at low angles of attack (up to $\alpha \approx 4$ deg), whereas the pitching moment is overestimated at all angles of attack. The same behavior is observed for the spanwise lift and pitching moment distributions, in Figs. 8a and 8b, obtained for a C_L of 0.316, a typical value for cruise conditions. As noted previously, the discrepancy in the pitching moment can be explained by the fact that in the Eulerian simulations the leading-edge suction peak is underestimated because of numerical errors. In this condition the flow is entirely subsonic,[12] so that the agreement between Eulerian results and experiments is expected to be qualitatively the same as in the $M = 0.3$ case.

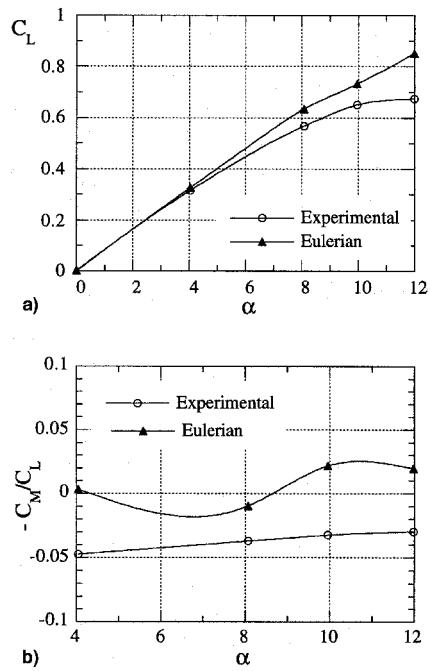

Fig. 7 Global values; $M = 0.7$: a) lift curve and b) estimation of the lift point of application.

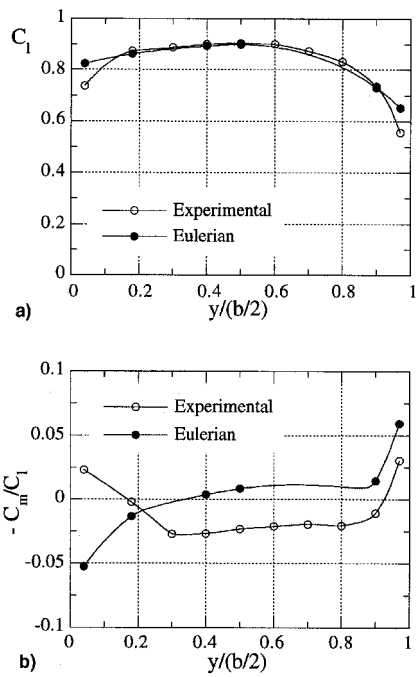

Fig. 6 Spanwise distributions; $M = 0.3$ and $C_L = 0.836$: a) lift distribution and b) estimation of the lift point of application.

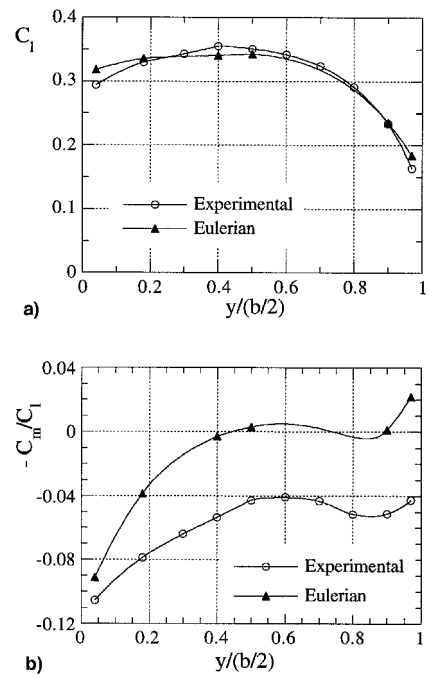

Fig. 8 Spanwise distributions; $M = 0.7$ and $C_L = 0.316$: a) lift distribution and b) estimation of the lift point of application.

For an angle of attack of 8 deg, the global lift coefficient is noticeably overestimated; in particular, the spanwise lift distribution in Fig. 9a shows that the discrepancy between Eulerian results and experiments is important in the inner region of the wing. For this angle of attack, the flow near the wing root is largely separated on the wing upper surface because of the strong boundary-layer/shock-wave interaction, as shown for instance by the experimental chordwise pressure distribution in Fig. 10a; consequently, it is clear that an Eulerian model cannot give accurate predictions in this region. Moreover, because the shock-wave position is strongly influenced by the separation of the boundary layer, the Euler simulation predicts a shock location noticeably different from the experiments, as shown in Fig. 10a. On the other hand, when the flow is not separated, a good agreement is found between the pressure distributions from Euler simulations and experiments, as shown, for example, in Fig. 10b [$y/(b/2) = 0.4$]. In particular, the shock-wave location is well predicted. Moreover, the CPU times and the number of iterations required in transonic computations are of the same order as in the subsonic case. This indicates that the numerical scheme is robust and efficient in capturing shock waves, as shown also in Ref. 2.

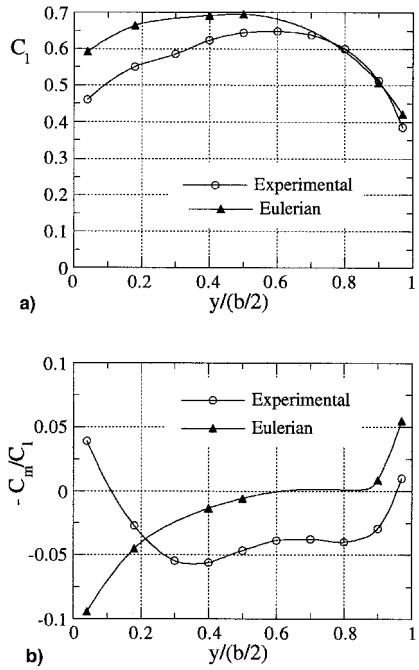

Fig. 9 Spanwise distributions; $M = 0.7$ and $\alpha = 8$ deg: a) lift distribution and b) estimation of the lift point of application.

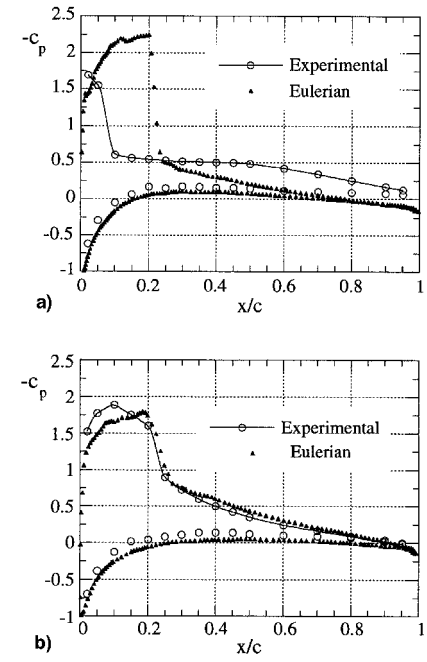

Fig. 10 Chordwise pressure distributions; $M = 0.7$ and $\alpha = 8$ deg. $y/(b/2)$ = a) 0.04 and b) 0.40.

Results of Navier–Stokes Simulations

Two different subsonic flow conditions have been considered for the Navier–Stokes simulations. The first one corresponds to a relatively low angle of attack ($\alpha = 8$ deg); for this case only laminar Navier–Stokes simulations have been carried out. In Fig. 11a the spanwise distributions of lift obtained from inviscid and viscous calculations are compared with the experimental data. As expected, because for this flow condition the boundary layer is not separated, the Euler and Navier–Stokes solvers have practically the same behavior. Nevertheless, the estimation of the lift point of application given by the Navier–Stokes solver is in better agreement with the experiments than that obtained from inviscid calculations (see Fig. 11b). This is a result of greater accuracy in the evaluation of the chord pressure distribution obtained near the trailing edge in the viscous simulations. Even if only a slight difference can be observed with Eulerian results, as can be seen in Fig. 12, this has a noticeable impact on the pitching moment evaluation. In Navier–Stokes simulations the suction peak at the leading edge is also underestimated, for the reasons explained in the previous section. The grid used for this case has 398,494 tetrahedral cells, and it has been obtained, starting from the grid used in Eulerian computation, by refining the zones of high-velocity gradient. The required CPU time is about 60 h. Moreover, a preliminary Navier–Stokes computation on a coarser grid is needed to obtain the final grid.

A more interesting case is represented by the flow at an angle of attack of 16 deg, when an important zone of separated flow has been observed in the experiments.[12] Because the extent of the separated zone is strongly affected by turbulence, in this case, the Reynolds-averaged equations with the standard k-ε model have also been considered. The grid used for the

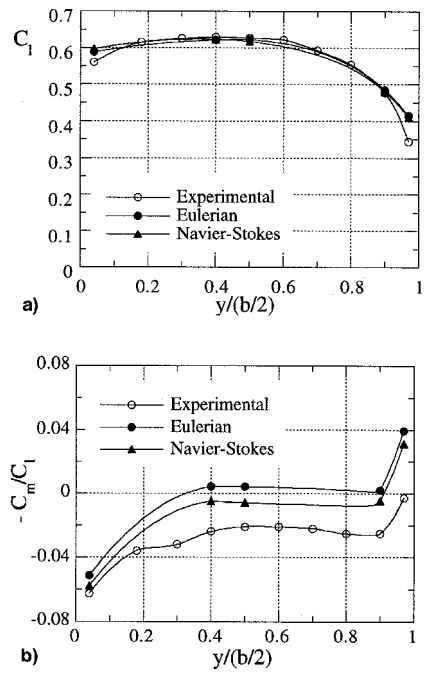

Fig. 11 Spanwise distributions; $M = 0.3$ and $C_L = 0.585$: a) lift distribution and b) estimation of the lift point of application.

laminar computation has a number of cells (357,194) comparable with that used at $\alpha = 8$ deg. For the turbulent computation an even more refined grid of 617,667 cells is needed to have an adequate resolution of the turbulent boundary layer.

Concerning the spanwise lift distribution shown in Fig. 13a, a better qualitative agreement with the experimental data is observed for both laminar and turbulent Navier–Stokes simulations, particularly at the wing root, even if, quantitatively, the agreement is still not noticeably improved. The lift point of application evaluated by both the Navier–Stokes solvers is also in better agreement with the experimental data than that obtained by the inviscid simulation (Fig. 13b). In particular, the best qualitative agreement is obtained with the turbulent computation, except at the wing root. Nevertheless, the laminar solver gives a more accurate quantitative evaluation. This is because the pressure distribution around the leading edge is better evaluated in the laminar case, as shown, for example, from the chordwise pressure distributions in Fig. 14. In the laminar case, even if the grid has a number of cells comparable with that used at $\alpha = 8$ deg and has been refined with the same criterion based on the velocity gradient, it is finer around the leading edge, as a consequence of the higher velocity gradient in this zone. This results in a good evaluation of the suction peak. On the other hand, in the k-ε model, the whole boundary layer is turbulent. Hence, in this model near the leading-edge region where the flow is laminar, the pressure is noticeably overestimated.

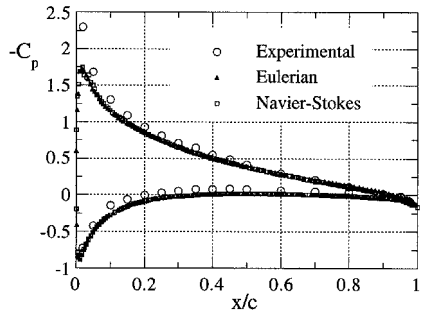

Fig. 12 Chordwise pressure distributions; $y/(b/2) = 0.4$, $M = 0.3$, and $\alpha = 8$ deg.

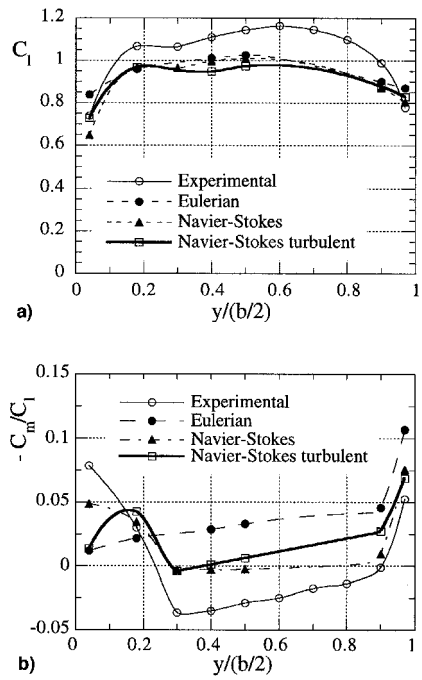

Fig. 13 Spanwise distributions; $M = 0.3$ and $\alpha = 16$ deg: a) lift distribution and b) estimation of the lift point of application.

For both viscous simulations a significant discrepancy is observed near the wing root in the evaluation of the lift point of application. In the laminar case this discrepancy most likely appears because in the simulation the separation line is found farther upstream than in the experiment, as shown from the chordwise pressure distribution in Fig. 14a. This result is not surprising because no turbulence model is used in the simulation. A better global agreement in pressure distribution is obtained with the k-ε model (Fig. 14a) and, in particular, the separation of the boundary layer seems to occur at the same location than in experiments. Nevertheless, the overestimation of the leading-edge pressure yields to a significant error in the evaluation of the lift application point. In Fig. 15, where the experimental and numerical separation lines are drawn, it is shown that the turbulent model gives a separation line close to the experimental one. As expected, in the laminar approximation, the separation is found more noticeably upstream. The experimental separation line is obtained from the liquid-crystal visualization, whereas the numerical one is estimated from the visualizations of the velocity field as shown in Fig. 16.

The required CPU time is about 85 h for the laminar case; for the turbulent computation the CPU time is three times larger than in the laminar simulation.

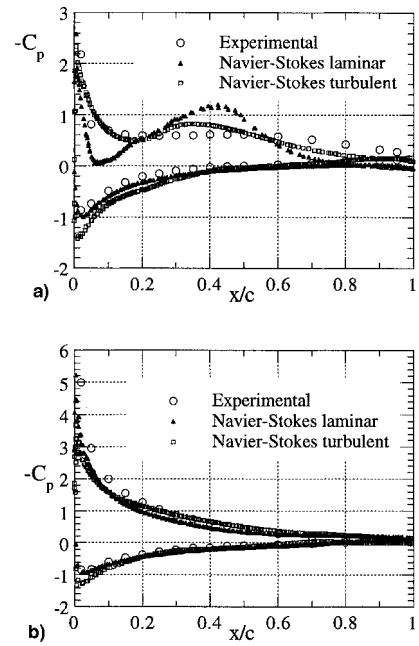

Fig. 14 Chordwise pressure distributions; $M = 0.3$ and $\alpha = 16$ deg. $y/(b/2)$ = a) 0.04 and b) 0.40.

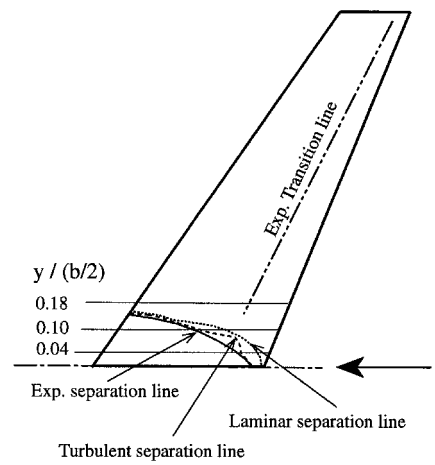

Fig. 15 Numerical and experimental separation lines; $M = 0.3$ and $\alpha = 16$ deg.

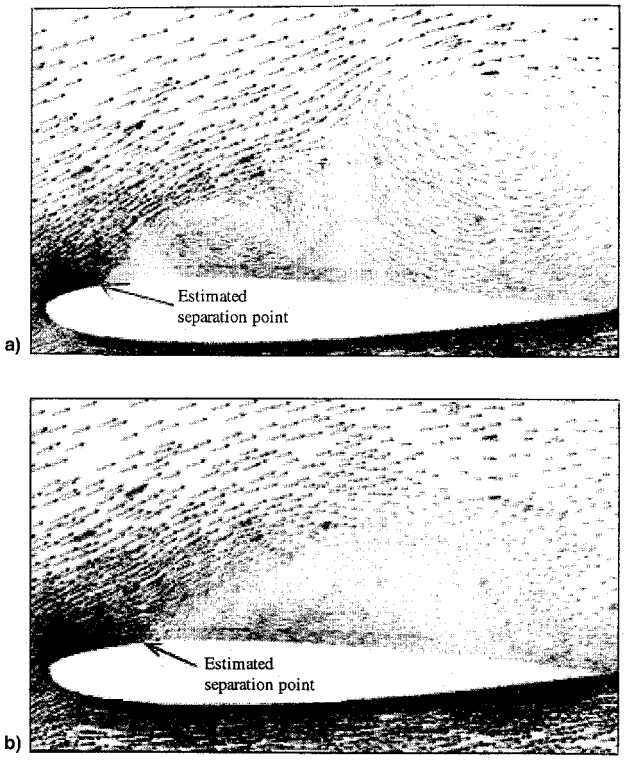

Fig. 16 Velocity field; $y/(b/2) = 0.04$, $M = 0.3$, and $\alpha = 16$ deg: a) laminar and b) turbulent flows.

Conclusions

The capabilities of different numerical methods in predicting the aerodynamics of forward-swept wings were investigated by comparing experimental data with numerical results. Both subsonic and transonic conditions were investigated.

In typical subsonic cruise conditions, when the limits of applicability of linear potential solvers are satisfied, these solvers correctly evaluate the lift- and pitching-moment distributions. It is interesting to remark that the agreement obtained with the Euler solver in the region around the leading edge, even with a very high-grid resolution, is less satisfactory. The CPU time and storage requirements are obviously noticeably larger for Euler calculations.

Increasing the angle of attack, because of the characteristics behavior of forward-swept wings, the vortical effects become more important and the increase in global lift with angle of attack is no longer linear. Potential solvers clearly cannot simulate correctly this type of flow, whereas the results show that the Euler solver is able to take these effects into account and give a satisfactory agreement with experimental data that is also in this regime. As the angle of attack is increased the flow is characterized by extended zones of boundary-layer separation, resulting in highly nonlinear effects. Clearly, an Eulerian solver cannot capture this type of nonlinearity. On the other hand, both laminar and turbulent Navier–Stokes solvers give a satisfactory prediction of lift and pitching moment distributions up to angles of attack characterized by extended zones of separated flow. Nevertheless, the prediction of the boundary-layer separation line obtained by the laminar model is not quantitatively accurate, as expected. In the simulation with the k-ε model a good evaluation of the extent of the separated zone is obtained. Nevertheless, because in this model the entire boundary layer is turbulent, a significant discrepancy is observed in the pressure distribution at the leading edge. In our opinion, the results could be improved in a model in which turbulent effects could be accounted for only in part of the boundary layer. Therefore, the analysis of current turbulence model capabilities, when a transition line is imposed, could be a further development of this research activity.

For transonic flow, the Eulerian solver shows good agreement with experimental results at angles of attack corresponding to cruise conditions. As the angle of attack increases, the boundary layer separates near the wing root and, clearly, this phenomenon cannot be predicted by the Euler solver. Moreover, the position and intensity of the shock wave, in this region, is strongly affected by viscous interactions. Thus, the Eulerian prediction of the shock-wave position and intensity is incorrect. On the contrary, the shock wave is well captured in the nonseparated regions.

Viscous flow simulations in transonic conditions require a deep analysis of the shock-wave/boundary-layer interaction and of the sensitivity to turbulence model. Because the flow visualizations for transonic flows are not yet available, a significant comparison cannot presently be done. Navier–Stokes transonic calculations will be presented together with the experimental visualizations in the future.

All of the numerical solvers gave results consistent with the physical limits of the equations that they discretized. In particular, when the basic physical assumptions are satisfied, the simplest methods give the same or even better accuracy than the more complex methods, with noticeably less cost and time requirements. It must be emphasized, however, that the evaluation of the limits of applicability of a specific numerical method is not trivial, particularly the physics of the flow is not known a priori.

Acknowledgment

We gratefully acknowledge the Centro Nazionale Universitario Calcolo Elettronico for providing the computing capacity.

References

[1]Morino, L., and Iemma U., "Boundary Integral Equations and Conservative Dissipation Schemes for Full Potential Transonic Flows," *Computational Mechanics*, Vol. 13, Nos. 1–2, 1993, pp. 90–99.

[2]Agraval, S., Creasman, S. F., and Lowrie, B. R., "Evaluation of Euler Solvers for Transonic Wing-Fuselage Geometries," *Journal of Aircraft*, Vol. 28, No. 12, 1991, pp. 885–891.

[3]Van Dam, C. P., Nikfetrat, K., Wong, K., and Vijgen, P. M. H. W., "Drag Prediction at Subsonic and Transonic Speeds Using Euler Methods," *Journal of Aircraft*, Vol. 32, No. 4, 1995, pp. 839–845.

[4]Woodson, S. H., and Campbell, J. F., "Interactive Three-Dimensional Boundary-Layer Method for Transonic Flow over Swept Wings," *AIAA Journal*, Vol. 29, No. 5, 1991, pp. 678, 679.

[5]Bonhaus, D. L., and Wornom, S. F., "Comparison of Two Navier-Stokes Codes for Attached Transonic Wing Flows," *Journal of Aircraft*, Vol. 29, No. 1, 1992, pp. 101–107.

[6]Tu, E. L., "Vortex-Wing Interaction of a Close-Coupled Canard Configuration," *Journal of Aircraft*, Vol. 31, No. 2, 1994, pp. 314–321.

[7]Agraval, S., and Vatsa, V. N., "Transonic Navier-Stokes Flow Computations over Wing-Fuselage Geometries," *Journal of Aircraft*, Vol. 30, No. 5, 1993, pp. 791–793.

[8]Kwon, O. J., and Lakshmi, N. S., "Viscous Flow Simulation of a Fighter Aircraft," *Journal of Aircraft*, Vol. 29, No. 5, 1992, pp. 886–891.

[9]Mavriplis, D. J., "Three-Dimensional Multigrid Reynolds-Averaged Navier-Stokes Solver for Unstructured Meshes," *AIAA Journal*, Vol. 33, No. 3, 1995, pp. 445–453.

[10]Ricketts, R. H., and Doggett, R. V., "Wind-Tunnel Experiments on Divergence of Forward-Swept Wings," NASA TP-1685, Aug. 1980.

[11]Buresti, G., Lombardi, G., and Morelli, M., "Pressure Measurements on Different Canard-Wing Configurations in Subsonic Compressible Flow," Atti del Dipartimento di Ingegneria Aerospaziale, ADIA 91-4, Sept. 1991.

[12]Lombardi, G., "Experimental Study on the Aerodynamic Effects of a Forward Sweep Angle," *Journal of Aircraft*, Vol. 30, No. 5, 1993, pp. 629–635.

[13]Lombardi, G., Morelli, M., and Waller, D., "Boundary Layer Transition on a Forward Swept Wing in Canard Configuration," *Journal of Aircraft*, Vol. 33, No. 6, 1996, pp. 1202–1204.

[14]Abid, R., and Vatsa, V. N., "Prediction of Separated Transonic Wing Flows with Nonequilibrium Algebraic Turbulence Model," *AIAA Journal*, Vol. 28, No. 8, 1990, pp. 1426–1431.

[15]Lombardi, G., and Morelli, M., "Analysis of Some Interference Effects in a Transonic Wind Tunnel," *Journal of Aircraft*, Vol. 32, No. 3, 1995, pp. 501–509.

[16]Lombardi, G., Morelli, M., and Waller, D., "Flow Visualization with Shear Sensitive Liquid Crystal—Some Examples and Problems," *Proceedings of the 7th International Symposium on Flow Visualization* (Seattle, WA), 1995, pp. 526–531.

[17]Polito, L., and Lombardi, G., "Calculation of Steady and Unsteady Aerodynamic Loads for Wing-Body Configurations at Subcritical Speeds," *Proceedings of Associazione Italiana di Aeronautica e Astronautica Conference* (Napoli, Italy), Vol. 1, 1983, pp. 209–222.

[18]Baston, A., Lucchesini, M., Manfriani, L., Polito, L., and Lombardi, G., "Evaluation of Pressure Distributions on an Aircraft by Two Different Panel Methods and Comparison with Experimental Measurements," 15th Int. Council of the Aeronautical Sciences Congress, London, Sept. 1986, pp. 618–628.

[19]"RAMPANT User's Guide," Release 3.1, Fluent, Inc., Lebanon, NH, July 1994.

[20]Roe, P. L., "Characteristic Based Schemes for the Euler Equations," *Annual Review of Fluid Mechanics*, Vol. 18, 1986, pp. 337–365.

[21]Devemport, W. J., and Simpson, R. L., "Flow Past a Wing-Body Junction-Experimental Evaluation of Turbulence Models," *AIAA Journal*, Vol. 30, No. 4, 1992, pp. 873–881.

[22]Milholen, W. E., II, and Chokani, N., "Effect of Sidewall Boundary Layer on Transonic Flow over a Wing," *Journal of Aircraft*, Vol. 31, No. 4, 1994, pp. 986–988.